SIMPLE TEST CASES WITH ACCURATE NUMERICAL SOLUTIONS FOR 3-D SOUND PROPAGATION MODELLING

Sven M. Ivansson[a]

[a]Swedish Defence Research Agency, SE-16490 Stockholm, Sweden

Sven M. Ivansson, Swedish Defence Research Agency, SE-16490 Stockholm, Sweden; fax +46 8 55503869; email sven.ivansson@foi.se

Abstract: *Modelling of sound propagation from a point source in media with azimuthal variations of bathymetry and/or sound speed is computationally challenging. The parabolic equation (PE) method is useful, but it entails approximations and verification by other methods is needed. By comparison with solutions by image source and adiabatic mode PE techniques, it has been realized in recent years that incorporation of a leading-order cross-derivative term in the PE square-root operator approximation is sometimes needed. Test cases of wedge and canyon type have been used, with medium variations in only one of the two horizontal Cartesian coordinates. For such media, the point-source solution can be expressed as an integral of solutions of an ensemble of 2-D problems. These 2-D problems can be solved by coupled modes, for example. In the present paper, a particular type of such test cases is considered. In essence, the difference of inverse squared sound speed at two arbitrary horizontal positions does not depend on depth. It follows that only the modal wavenumbers depend on horizontal position, not the mode shapes. The pertinent ensemble of 2-D problems can be solved separately for each mode, and the "adiabatic approximation" is thus exact. Direct propagator-matrix multiplication, from opposite horizontal directions with matching at the source range, is applied to obtain explicit solutions in terms of exponential and Airy functions, and the pertinent integral is computed with error control using adaptively determined step lengths. Two specific examples are studied in detail, one of "wedge" type and one of "canyon" type. Despite the simplifications made, allowing very accurate numerical solutions, clear mode-dependent effects of horizontal refraction are obtained and compared to modal ray diagrams. Comparisons with 3-D PE results are under way.*

Keywords: *Normal mode, wavenumber integration, adiabatic approximation*

1. INTRODUCTION AND SUMMARY

The parabolic equation (PE) method is useful for modelling 3-D sound propagation, but approximations are involved and comparisons with results by different methods are needed. A truncated wedge with a homogeneous water layer overlying a homogeneous sediment half-space has been a popular test case, and a canyon alternative with a Gaussian bathymetry has also been studied [1]. Image source and adiabatic mode PE methods have been used for verification [1],[2],[3],[4].

In the present paper, test cases are considered for which the lateral variation is caused by sound-speed rather than bathymetry changes. As with the mentioned wedge and canyon cases, the medium variation is restricted to one of the two Cartesian horizontal coordinates, x. By Fourier transformation with respect to the other horizontal coordinate, y, the 3-D problem can be solved by integrating solutions of 2-D problems, e.g., [5]. As in Sec. 3.6.1 of [6] and Sec. 3 of [7], the inverse squared sound speed is assumed to be expressible as the sum of a function depending on depth z and a function of x. It follows that the 2-D problems can be solved separately for each mode (the adiabatic approximation is exact).

After some theory in Sec. 2, a range-invariant reference case is considered in Sec. 3. Secs. 4 and 5 deal with examples related to the previously used wedge and canyon cases, respectively. High sound velocities are allowed to produce clear 3-D effects in the very accurate numerical solutions. Comparisons to approximate PE results are in progress.

2. THEORY

A Cartesian xyz coordinate system is introduced with x, y, z increasing to the east, north, and downward, respectively. There is a fluid medium with density $\rho(z)$ and sound speed $c(x,z)$ between a free surface at $z = 0$ and an artificial free or rigid bottom at $z = z_h > 0$. A symmetric acoustic point source with harmonic time dependence according to the typically omitted factor $\exp(-i\omega t)$, where $\omega > 0$ is angular frequency and t is time, appears at $z = z_s$ on the z axis. Since ρ only depends on z and c is independent of y, the Helmholtz equation for the acoustic pressure p takes the form

$$\frac{\partial^2 p}{\partial x^2} + \rho(z)\frac{\partial}{\partial z}\left(\frac{1}{\rho(z)}\frac{\partial p}{\partial z}\right) + \frac{\partial^2 p}{\partial y^2} + \left(\frac{\omega^2}{c^2(x,z)}\right)p = \left(\frac{\omega^2}{c^2(x,z)}\right)M\delta_s\,, \tag{1}$$

where δ_s is the 3-D Dirac function centred at $(x,y,z) = (0,0,z_s)$ and M is the moment-tensor strength of the source. Fourier transformation of Eq. (1) shows that

$$p(x,y,z) = \int_{-\infty}^{+\infty} \hat{p}(x,z;\kappa)\ e^{i\kappa y}\,d\kappa\,, \tag{2}$$

where, for each κ, $\hat{p}(x,z;\kappa) = (2\pi)^{-1}\int_{-\infty}^{+\infty} p(x,y,z)\ e^{-i\kappa y}\,dy$ fulfils the 2-D Helmholtz equation

$$\frac{\partial^2 \hat{p}}{\partial x^2} + \rho(z)\frac{\partial}{\partial z}\left(\frac{1}{\rho(z)}\frac{\partial \hat{p}}{\partial z}\right) + \left(\frac{\omega^2}{c^2(x,z)} - \kappa^2\right)\hat{p} = \left(\frac{\omega^2}{c^2(x,z)}\right)\frac{M\delta(x)\delta(z-z_s)}{2\pi} \tag{3}$$

Here, δ is the 1-D Dirac function. The problem is thereby reduced to numerical integration of the solutions to a number of κ–dependent 2-D problems. A resonance phenomenon

appears when κ is equal to a modal wavenumber for a specific laterally homogeneous region. Hence, for a medium with vanishing or very small absorption, the integration path must in general be displaced from the real axis into the lower half-plane.

Restriction is now made to sound-speed profiles $c(x,z)$ such that

$$\frac{1}{c^2(x,z)} = \frac{1}{c_0^2(z)} + S(x) \,, \tag{4}$$

where $c_0(z) = c(0,z)$ and $S(x)$ is a continuous and piece-wise linear function of x such that $S(0) = 0$ and $S(x)$ is constant for large positive x and large negative x as well.

By separation of variables, it follows that Eq. (3) is solved by

$$\hat{p}(x,z;\kappa) = \sum_{m=1}^{\infty} h_m(x;\kappa) Z_m(z) \,, \tag{5}$$

where the Z_m are mode functions with modal wavenumbers $k_{m,0}$ fulfilling

$$\rho(z)\frac{\mathrm{d}}{\mathrm{d}z}\left(\frac{1}{\rho(z)}\frac{\mathrm{d}Z_m}{\mathrm{d}z}\right) + \left(\frac{\omega^2}{c_0^2(z)} - k_{m,0}^2\right) Z_m = 0 \tag{6}$$

and the h_m are coefficient functions fulfilling

$$\frac{\partial^2 h_m}{\partial x^2} + (k_m^2(x) - \kappa^2) h_m = \left(\frac{\omega^2}{c^2(0,z_\mathrm{s})}\right) \frac{M Z_m(z_\mathrm{s}) \delta(x)}{2\pi\rho(z_\mathrm{s}) I_m} \tag{7}$$

with $k_m(x) = \left(k_{m,0}^2 + \omega^2 S(x)\right)^{1/2}$ and $I_m = \int_0^{z_\mathrm{h}} \rho^{-1}(z) Z_m^2(z)\,\mathrm{d}z$. Together with the appropriate boundary conditions, Eqs. (6) and (7) can be solved by propagator-matrix techniques as detailed in Secs 3.3.2 and 3.2.1.2 of [6], for example.

3. A LATERALLY HOMOGENEOUS REFERENCE CASE

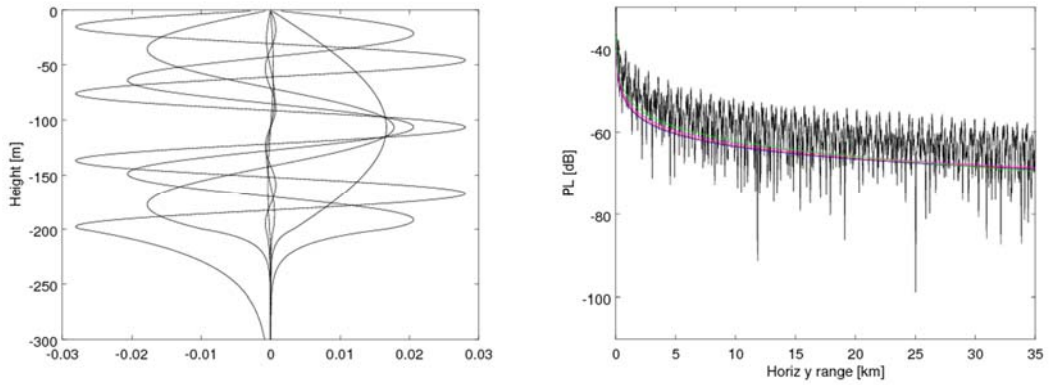

Fig.1: Mode shapes at 30 Hz as excited by a source at depth 106 m (left). Modes 1, 3, 5, 7 are strong at depth 106 m, while modes 2, 4, 6 are weak there. The right panel shows corresponding PL curves at (x,z) = (0,106) m: including all seven modes (black), and for each of modes 1, 3, 5, 7 separately (blue, red, magenta, green).

A homogeneous 200 m deep water column with sound speed 1500 m/s is overlying a homogeneous fluid sediment half-space with sound speed 3000 m/s, absorption 0.1 dB/wavelength and density 1500 kg/m^3. For technical reasons, the half-space is truncated

by a free boundary at depth, with a gradual absorption increase with depth towards this boundary to prevent reflections from it. The sound source appears at $(x,y,z) = (x_s,y_s,z_s) = (0,0,106)$ m, as in all examples to follow. The right panel of Fig. 1 shows propagation loss (PL) at the receiver depth 106 m for the field contribution by the first seven modes. The left panel shows the mode shapes, as excited. Modes 1, 3, 5, 7 dominate.

Fig. 2 shows corresponding time traces including modes 1-5 for a pressure pulse with amplitude spectrum concentrated to the band 28-40 Hz. Mode 1 arrives first, at reduced time $t - y/c$ close to zero, where $c = 1.5$ km/s, and the highly dispersive modes 3 and 5 follow. It is helpful for the mode identification to plot time traces at various receiver depths for fixed ranges. This is done for $(x,y) = (0,20)$ km in Fig. 3. At $y = 20$ km, modes 3 and 5 apparently arrive at reduced times about 0.5 and 1.5 s, respectively.

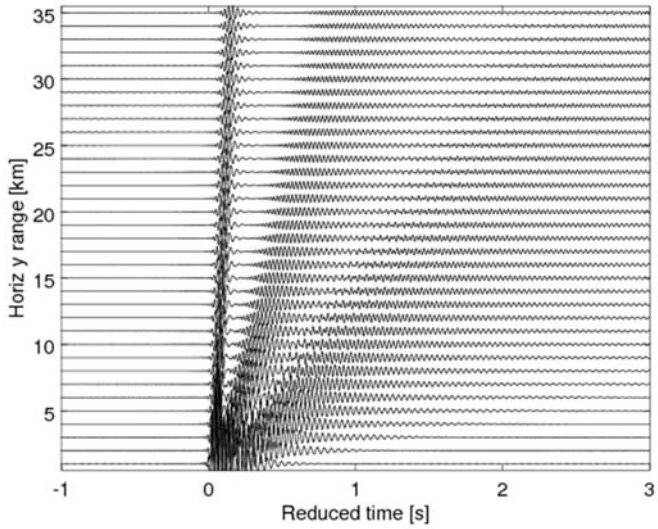

Fig.2: Time traces at (x,z) = (0,106) m for y = 1,2,..,25 km.

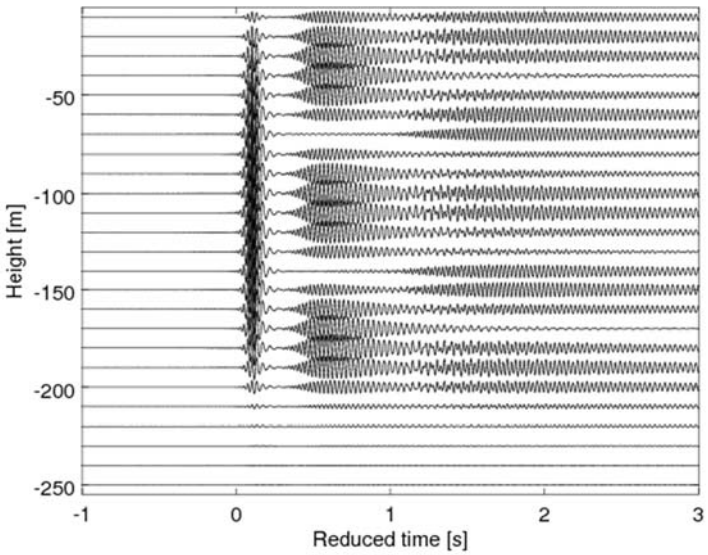

Fig.3: Time traces as in Fig. 2 but at (x,y) = (0,20) km for z = 10,20,..,250 m.

4. AN EXAMPLE OF WEDGE TYPE

The medium example from Sec. 3 is now modified by introducing a non-vanishing $S(x)$ according to Eq. (4). Specifically, $S(x)$ is constant in $x < -3.6$ km, and it is linear in -3.6

km < x < 2.8 km as well as in 2.8 km < x < 3.6 km. As indicated by the left panel of Fig. 4, the corresponding "water" sound speed is 1600 m/s at x = 2.8 km and 1700 m/s at $x \geq 3.6$ km. The right panel of Fig. 4 shows the corresponding "sediment" sound speed.

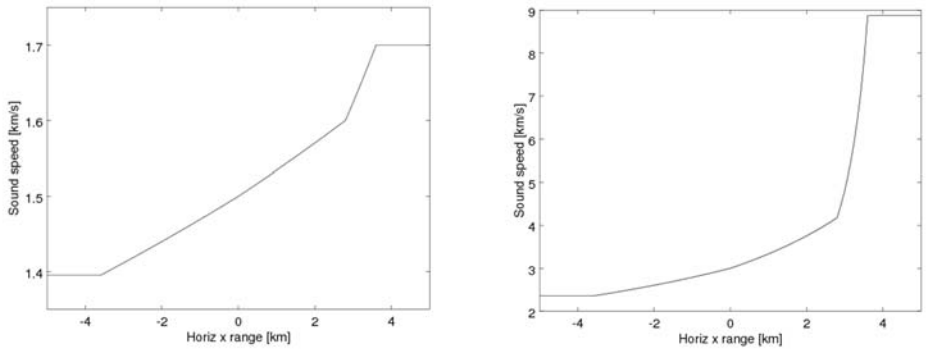

Fig.4: Wedge-type case with "water" (left) and "sediment" (right) sound speed.

The left panel of Fig. 5 shows PL curves corresponding to those in the right panel of Fig. 1, with significant effects of horizontal refraction. These effects may be illustrated nicely by modal ray diagrams [8],[1], see the right panel and Fig. 6.

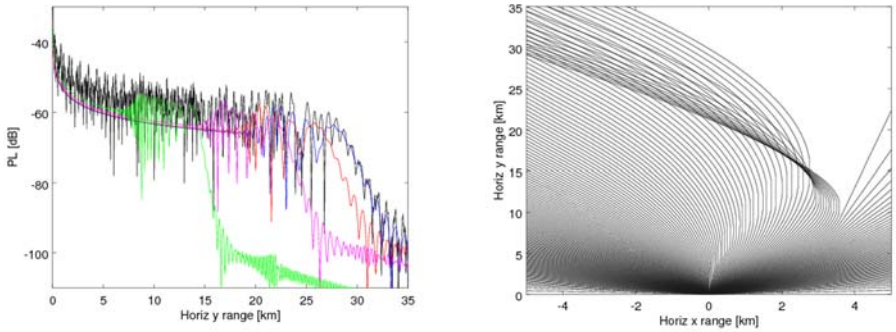

Fig.5: PL curves as in the right panel of Fig. 1 but for the wedge example (left). The right panel shows horizontal rays for mode 1.

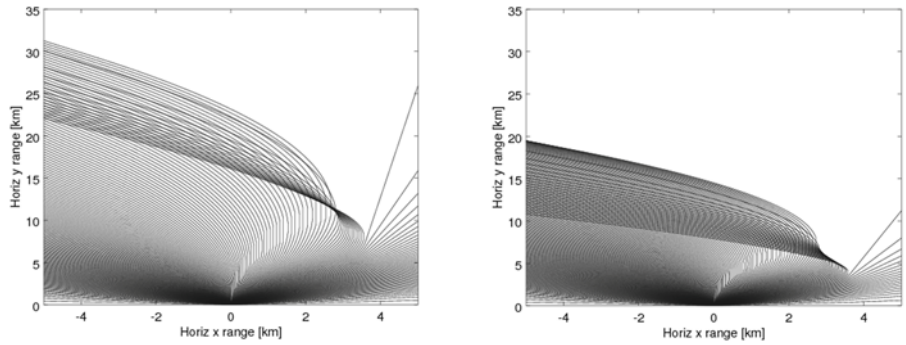

Fig.6: Horizontal rays as in Fig. 5, right panel, but for modes 5 (left) and 7 (right).

Broad-band results, corresponding to those in Fig. 2, appear in Fig. 7. At some y ranges there are two arrivals for each of the modes 1, 3, and 5, cf. the modal ray diagrams. Their interference gives rise to a characteristic beat pattern for the dispersive modes 3 and 5.

Fig. 8 shows time traces at various depths at y = 19 km. At this y range, there is multi-pathing only for mode 5. At y = 22 km, see Fig. 9, all of modes 1, 3, 5 exhibit multi-pathing.

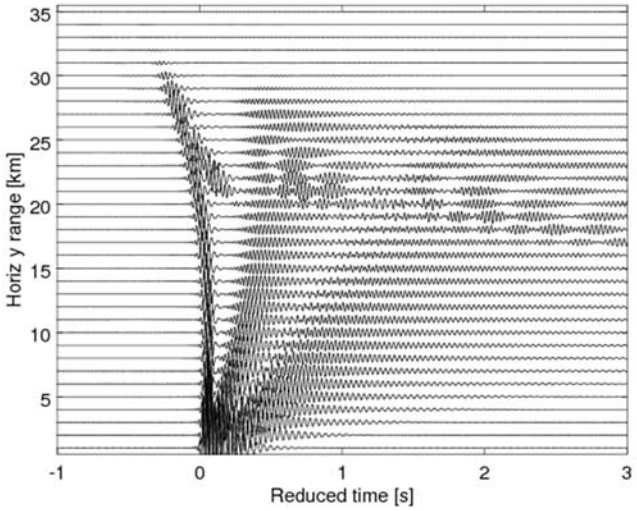

Fig.7: Time traces as in Fig. 2 but for the wedge case.

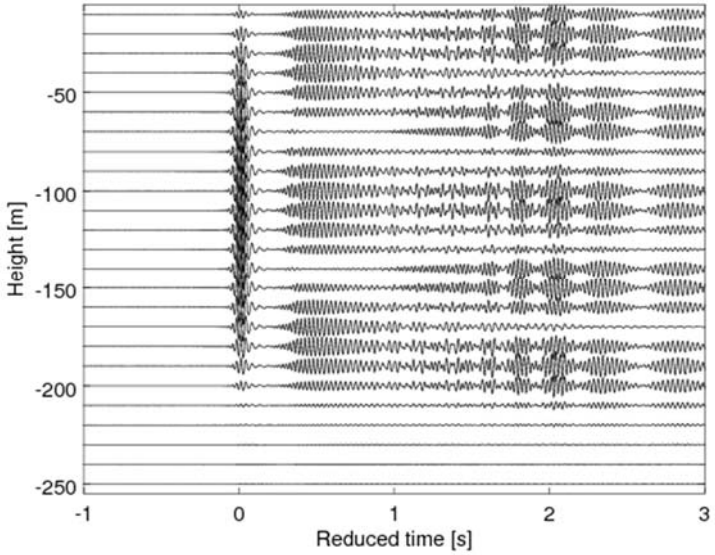

Fig.8: Time traces as in Fig. 7 but at (x,y) = (0,19) km for z = 10,20,..,250 m.

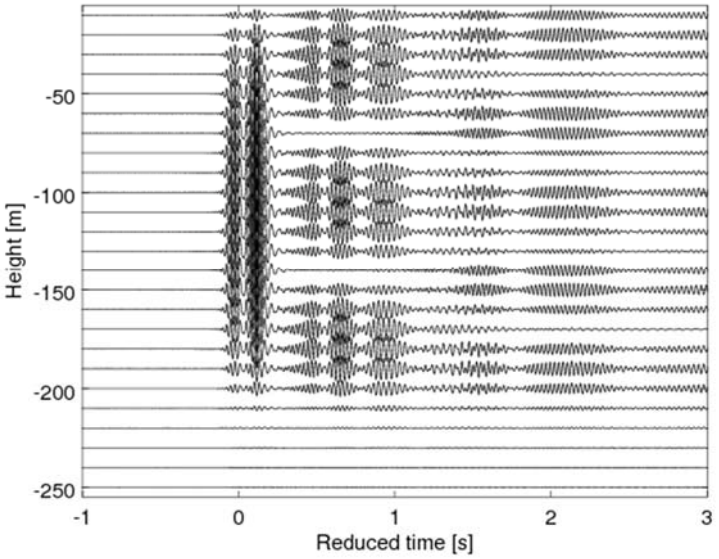

Fig.9: Time traces as in Fig. 8 but at (x,y) = (0,22) km.

5. AN EXAMPLE OF CANYON TYPE

The positive-x part of the $S(x)$ function from Sec. 4 is now mirrored in the y axis. A canyon-type example appears, with "water" and "sediment" sound speeds as in Fig. 10.

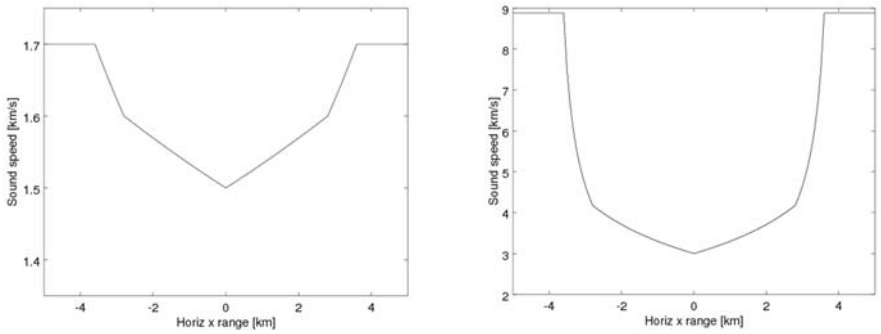

Fig.10: Canyon-type case with "water" (left) and "sediment" (right) sound speed.

This time, many horizontal mode rays get trapped in the canyon, bouncing back and forth there, cf. the modal ray diagrams in Fig. 12. Thus, see the PL results in Fig. 11, the horizontal refraction causes increased pressure levels as compared to the range-invariant case. The individual modes contribute significantly over the whole range interval. For the third mode, significant interference between paths with clearly different travel times starts at about y = 20 km, cf. Fig. 13.

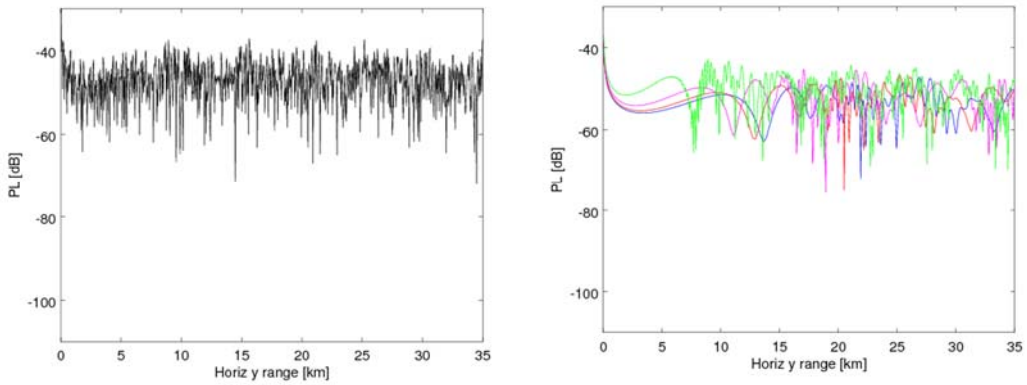

Fig.11: PL curves as in the right panel of Fig. 1 but for the canyon example, including all seven modes (left; black) and each of modes 1, 3, 5, 7 separately (right; blue, red, magenta, green).

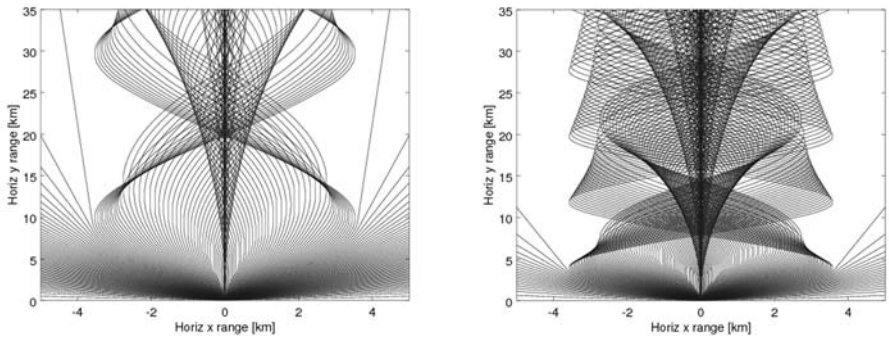

Fig.12: Horizontal rays for modes 3 (left) and 7 (right).

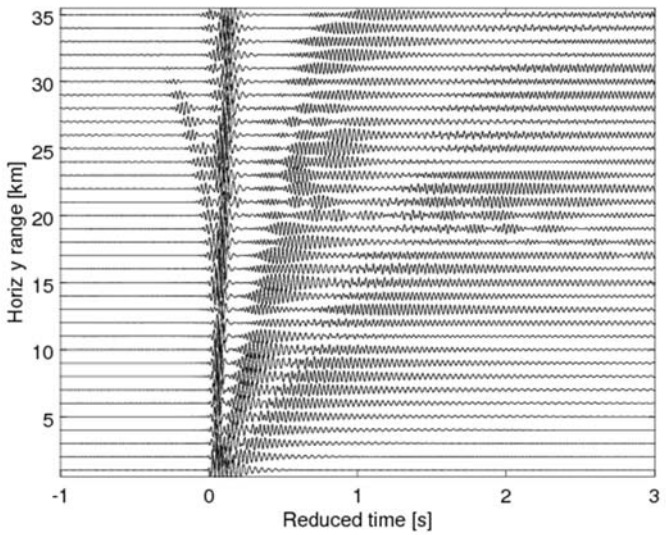

Fig.13: Time traces as in Fig. 2 but for the canyon case.

REFERENCES

[1] **F. Sturm**, Numerical study of broadband sound pulse propagation in three-dimensional oceanic waveguides, *J. Acoust. Soc. Am.*, 117 (3), pp. 1058-1079, 2005.

[2] **Y.-T. Lin, J.M. Collis, T.F. Duda**, A three-dimensional parabolic equation model of sound propagation using higher-order operator splitting and Padé approximants, *J. Acoust. Soc. Am.*, 132 (5), pp. EL364-EL370, 2012.

[3] **F. Sturm**, Leading-order cross term correction of three-dimensional parabolic equation models, *J. Acoust. Soc. Am.*, 139 (1), pp. 263-270, 2016.

[4] **P.S. Petrov, F. Sturm**, An explicit analytical solution for sound propagation in a three-dimensional penetrable wedge with small apex angle, *J. Acoust. Soc. Am.*, 139 (3), pp. 343-1352, 2016.

[5] **J.A. Fawcett, T.W. Dawson**, Fourier synthesis of three-dimensional scattering in a two-dimensional oceanic waveguide using boundary integral integration methods, *J. Acoust. Soc. Am.*, 88 (4), pp. 1913-1920, 1990.

[6] **S. Ivansson**, Sound propagation modelling, In *Applied Underwater Acoustics*, L. Bjørnø, T. Neighbors, D. Bradley (Eds.), Elsevier, pp. 185-272 (Chap. 3), 2017.

[7] **S. Ivansson**, Simple illustrations of range-dependence and 3-D effects by normal-mode sound propagation modelling, In *Proc. 39th Scandinavian Symposium on Physical Acoustics*, Geilo, Norway, 2016.

[8] **J.A. Fawcett**, Modeling three-dimensional propagation in an oceanic wedge using parabolic equation methods, *J. Acoust. Soc. Am.*, 93 (5), pp. 2627-2632, 1993.